Hindawi
International Journal of Aerospace Engineering
Volume 2023, Article ID 2451808, 11 pages
https://doi.org/10.1155/2023/2451808

Research Article

Investigation of the Effect of Axial Gap on the Mechanical Response of a Cartridge-Loaded CMDB Propellant Grain under Vibration Loads

Yiming Zhang,[1] Ningfei Wang,[1] Xiaoxu Chen,[1] Ran Wang,[1] Long Bai,[1] Jinfeng Dang,[2] and Yi Wu[1]

[1]*School of Aerospace Engineering, Beijing Institute of Technology, Beijing 100081, China*
[2]*Xi'an Modern Control Technology Research Institute, Xi'an 710065, China*

Correspondence should be addressed to Yi Wu; yi.wu@bit.edu.cn

Received 20 August 2022; Revised 26 April 2023; Accepted 31 May 2023; Published 15 June 2023

Academic Editor: Qingfei Fu

In this study, the effect of the axial gap on the mechanical response of a cartridge-loaded propellant grain under vibration loads is investigated. The wide strain rate range of uniaxial compression tests ($1.7 \times 10^{-3} \sim 4 \times 10^{3}\ s^{-1}$) on the composite modified double base (CMDB) propellant was carried out by using a universal testing machine, a hydraulic testing machine, and a split Hopkinson pressure bar system, respectively. A linear viscoelastic constitutive model of the CMDB propellant was developed by using the experimental measurements. The results show the studied CMDB propellant has a strong strain rate dependence, exhibiting an initial linear elasticity followed by a strain hardening region. The dynamic process of collision between the propellant grain and the motor case in the axial direction induced by vibration loads was simulated with the developed constitutive model by using the finite element method. The effects of the gap size between the propellant grain and the case and the vibration frequency on the mechanical response of the grain were studied. This shows that with a constant vibration frequency, the stress of the grain increases first and then decreases with increasing gap size. Moreover, the stress increases with increasing vibration loads.

1. Introduction

In solid rocket motors (SRMs), one of the methods of holding the grain in the case is using cartridge-loaded propellant grains [1–6]. In cartridge-loaded solid rocket motors, the propellant grains are manufactured separately from the case and then loaded into or assembled into the case. The propellant grain is normally fixed by the forward and backwards support inside motor cases [7–11]. The cartridge-loaded SRM has the advantage of low cost and ease of inspection and is commonly used in small missiles and a few medium-sized motors [12–14]. However, due to temperature variation, aging, and other issues, the size of the propellant grain could decrease gradually, leading to an axial gap between the propellant grain and the support [15–17]. This gap causes the propellant grain and the support gasket to collide with each other under vibration conditions, possibly resulting in the destruction of the structural integrity of the propellant grain. The vibration load during the transport subjected to the propellant has a certain periodicity, and the stress and strain of grain may exceed the capacity range of the solid propellant causing crack propagation in the propellant [18, 19]. These cracks can lead to the ignition failures of grain and even the explosion of the solid rocket motor. Therefore, it is important to evaluate the effect of the axial gap on the mechanical response of cartridge-loaded solid propellant grains under vibration loads.

Composite-modified double-base propellants (CMDBs) have been widely used in cartridge-loaded SRMs, owing to their excellent properties of low characteristic signals, good combustion performance, and exceptional processability [7, 20, 21].

CMDB propellant is a polymer composite material filled with a certain number of solid granules. The mechanical properties of the CMDB propellant have a great dependency on the strain rate [16, 22–25]. For a comprehensive understanding of the effect of the axial gap on the mechanical response of the CMDB propellant grain under vibration conditions, the deformation of the solid propellant material and the vibration conditions to which the propellant grain is subjected should be modelled accurately. A resume of literature reveals that there have been various studies to investigate the reliability of solid propellants under vibration loads [26–30]. For instance, Yilmaz et al. presented a methodology considering damage accumulation for the assessment of the service life of SRMs under random storage and transportation loads [18]. Kohsetsu proposed a simplified method to generate the structural vibration model of an SRM based on the mixed finite element method (M-FEM) for the analysis of carrier rocket vibration [31]. Kunz built a type of linear cumulative damage (LCD) model of a solid propellant under a variety of loading histories [32]. Zhang et al. used pavement inequality excitation to calculate the vibration response of an SRM by numerical simulation [33]. Cao et al. studied the structural integrity in the process of SRM launching and transporting by the vibration data monitored on the practical transport process of SRMs [34]. Huang and Zhang analyzed the effects of temperature and low-frequency vibration loads on the stress and strain of SRMs based on monitored temperature and vibration data [35].

The aforementioned studies of vibration load subjected to solid propellants are mainly about the reliability, vibration test, and new damage constitutive model development of solid propellants [17, 32, 36, 37]. However, mechanical response analysis for cartridge-loaded CMDB propellant grains with axial gaps under vibration loads has rarely been studied. To better understand the collision process caused by the gap between the case and the propellant grain under vibration loads, not only is the viscoelastic constitutive model of the propellant capable of accurately predicting the mechanical behavior of the propellant over a wide range of strain rates needed, but the influence of the vibration frequency and gap size on the collision process also needs to be studied.

Therefore, the objective of the present work is to investigate the effect of the axial gap on the mechanical response of a cartridge-loaded CMDB propellant grain under different vibration conditions. First, a linear viscoelastic constitutive model of the CMDB propellant was developed based on axial compression measurements conducted over a large range of strain rates. Then, the dynamic collision process of a cartridge-loaded propellant grain under vibration loading was simulated by using the developed constitutive model with the finite element method. The dynamic stress–strain distribution of the grain was obtained. The effects of the axial gap between the case and the propellant grain and the vibration frequency on the stress response of the propellant grain were discussed in detail.

2. Methodology

2.1. Material Properties. The components of the CMDB propellant studied in the present work are shown in Table 1. The nitrocellulose (NC) and nitroglycerin (NG) of the propellant are used as a double base binder, cyclotetramethylene tetranitramine (HMX) is used as an oxidizer, and the others are used as additives, including lead/copper-based compound salt as a combustion catalyst and dimethyl diphenylurea as a stabilizer. The mean size of the HMX particles used is approximately 90 μm. The degree of esterification of the NC is approximately 11.9%. Figure 1 shows the microstructure of the CMDB propellant, indicating that the HMX filler is homogeneously distributed in the binder matrix. Before the test, all specimens were stored in a vacuum oven at 20°C for 24 h to eliminate the residual stress and humidity of the propellant.

Table 1: Components of CMDB propellant.

Component	NC	NG	HMX	Other additives
Content (wt%)	50	32	10	8

2.2. Cartridge-Loaded Solid Motor. In this paper, the solid rocket motor studied is a cartridge-loaded type with an end-burning propellant grain, as shown in Figure 2. The solid rocket motor consists of a motor case, an end propellant grain, the insulation, and the motor case.

The motor case of the solid motor is made of steel material with a thickness of 4 mm, which is considered an elastic material. To study the effect of gap size on the collision process, the axial gap between the case and the propellant grain is prospectively set to 0 mm, 0.3 mm, $\pi/2 - 1$ mm, 1 mm, 2 mm, 3 mm, π mm, 4 mm, 5 mm, $3/2\,\pi + 1$ mm and 2π mm. Table 2 lists the mechanical properties of the case and grain used in the simulation. The geometrical details of the motor case and the propellant grain are shown in Table 3.

2.3. Numerical Setup

2.3.1. Constitutive Model. CMDB propellants are a type of particle-filled polymer composite material. The mechanical properties of the CMDB propellant are affected by the strain rate. As the collision process between the propellant grain and the motor cases is a typical dynamic impact issue, an accurate constitutive model of propellant grain under dynamic conditions must be first established. Assume that the propellant is homogeneous and linear viscoelastic. The Poisson ratio of propellant is constant. In the present work, the Prony series constitutive model applied a wide strain rate was established by using the data of uniaxial compression tests at a wide strain rate ($1.7 \times 10^{-3} \sim 4 \times 10^{3}\ \mathrm{s}^{-1}$).

The results of uniaxial compression tests show that the CMDB propellant exhibits linear mechanical behavior before the yield point. Therefore, a single integral linear viscoelastic constitutive model which is based on the Boltzmann superposition principle and generalized Maxwell model is used to describe the stress–strain behavior before the yield point of the CMDB propellant. The formula of the constitutive model used in the study is

$$\sigma(\mathrm{t}) = \int_0^t E(t-\tau)\,\frac{\partial \varepsilon}{\partial \tau}\,d\tau. \tag{1}$$

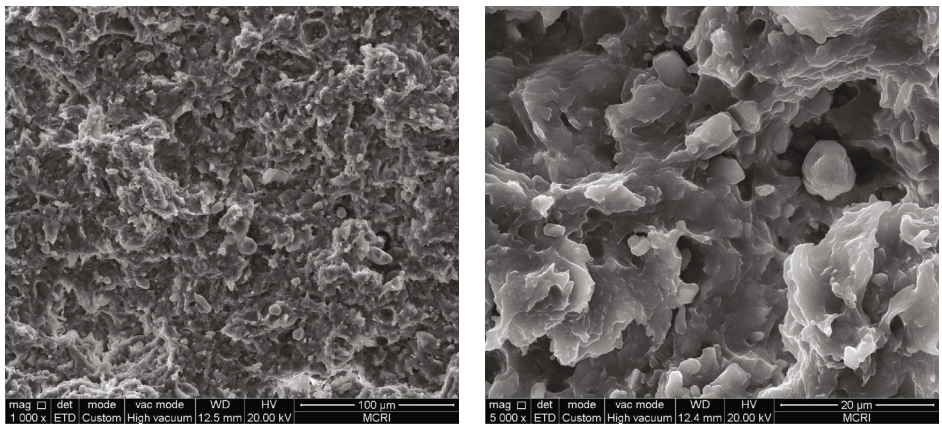

(a) ×1000 (b) ×5000

Figure 1: Microstructure of the CMDB propellant. (a) ×1000 magnification and (b) ×5000 magnification.

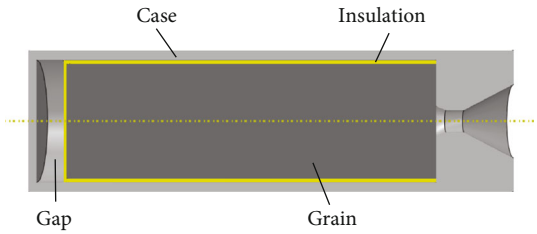

Figure 2: The structure of the studied solid rocket motor.

Table 2: Material properties of the motor case and propellant grain.

Part	Density (kg/m3)	Elasticity modulus [MPa]	Poisson's ratio
Case	7.85×10^3	210000	0.3
Grain	1.75×10^3	—	0.495

Table 3: Basic dimensions of the studied SRM.

Part	Inner diameter (mm)	Outer diameter (mm)	Length (mm)
Grain	50	—	215
Case	52	60	228

$\sigma(t)$ is the true stress, and $E(t)$ is the elastic modulus. In the developed constitutive model, the elastic modulus E is usually expressed in the form of a Prony series.

$$E(t) = E_\infty + \sum_{i=1}^{n} E_i e^{-t/\theta_i}. \quad (2)$$

E_∞ is the equilibrium modulus; E_i and θ_i are the modulus and relaxation time of each Prony series component.

The constitutive model of the CMDB propellant before the yield point is

$$\sigma = E_\infty \varepsilon + \sum_{i=1}^{n} E_i \dot{\varepsilon} \theta_i \left(1 - \exp\left(-\frac{\varepsilon}{\theta_i \dot{\varepsilon}}\right)\right). \quad (3)$$

It is considered that the propellant specimen deforms at a constant strain rate in the uniaxial compression test.

2.3.2. Basic Assumptions and Meshing. First, the following approximations have been made. In the present work, the energy loss caused by the collision and the effect of the temperature change caused by the collision are not considered in the simulation. The contact surfaces between the case and the propellant grain are set as frictionless. To improve the computational efficiency, in our simulation, the geometry of the studied solid rocket motor was simplified to an asymmetric two-dimensional model consisting only of the motor case and the propellant grain, as illustrated in Figure 3.

The uniform structure quadrilateral mesh is used into the grain and case. Precalculations with mesh sizes of 0.5 mm, 1 mm, and 1.5 mm are initially carried out to make sure the mesh size is small enough for an accurate calculation. Figure 4 shows the displacement of the propellant grain's top center at various mesh sizes. The axial displacement curves obtained using three different mesh sizes are very similar, illustrating that the mesh size between 0.5 and 1.5 mm is tiny enough to obtain accurate results. The propellant grain mesh size is set to 1 mm for all the conditions described in the next sections. The mesh of the case is divided more finely with a size of 0.5 mm. The number of propellant grain's total elements is 4480, and the number of motor case's total element is 5375 potentially. It should be noted that the insulation is not considered in our simulations. If the insulation is considered, the calculated von Mises stress will decrease due to the cushion action of insulation. However, the existence of insulation will not change the tendency of the effects of the gap size and vibration frequency. Therefore, the insulation was not considered in the simulation model.

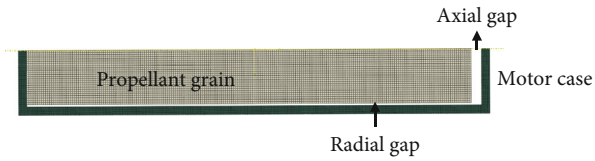

Figure 3: Schematic of grid block division unit.

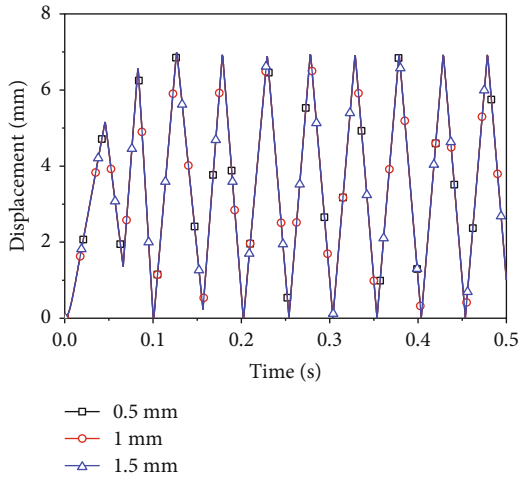

Figure 4: Displacement curves of the top center of the grain under different mesh sizes.

2.3.3. Boundary and Load Conditions. In our simulation, the vibration load is achieved by adding a periodic movement of the motor casing impacting the fuel grain. The periodic displacement applied to the case follows the equation below:

$$x(t) = A - A\cos(2\pi f t). \tag{4}$$

A and f are the amplitude and frequency of the vibration, respectively. The displacement curve of the case is shown in Figure 5. In the whole vibration process, the motor case drives the propellant grain to move. By simulating the motion of the grain and the motor case under vibration load, the stress of the contact surfaces between the grain and the case in the collision process is calculated.

2.4. Uniaxial Compression Experiments. To establish the constitutive model of the CMDB propellant suitable for simulating the mechanical response of the propellant grain under vibration loads. A split Hopkinson pressure bar, an Instron VHS 160/100-20 high-speed hydraulic servo testing machine, and an Instron 4505 universal testing machine were used to carry out uniaxial compression tests of the CMDB propellant at low, medium, and high strain rates. A wide range of strain rate uniaxial compression tests of the CMDB propellant were performed. The measurement matrix of the strain rate is outlined in Table 4. Each strain rate test was performed at least five times to confirm its correctness and reliability, and the average of those results served as the final experimental measurement values.

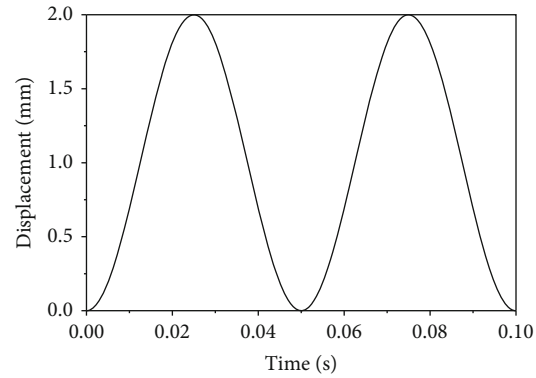

Figure 5: The displacement of the motor case.

The specimens were produced as 16 mm in diameter and 20 mm in length in the low strain rate compression tests. In order to remove any variability in the results brought by the selection of dimensions, the specimens in the intermediate strain rate tests with dimensions identical to those used for low strain rate compression testing were tested. Figure 6(a) depicts the intermediate strain rate compression testing device and specimens. The specimens had a diameter of 10 mm and a length of 5 mm, and they were cylindrical for the high strain rate compression test. The length-to-diameter ratio was designed as 0.5. Figure 6(b) shows a schematic representation of the intermediate strain rate compression testing device and specimens. By such a design, it can minimize wave attenuation in the strain signals recorded [16, 38] and the effects of radial and longitudinal inertia in the specimen [39]. The CMDB propellant which was used in all tests was in its original state. In our earlier study by Yang et al., the hydraulic testing device that was used here is described in great detail. [25].

3. Results and Discussion

3.1. Compression Test. The obtained stress–strain curves of the CMDB propellant under different strain rates are shown in Figure 7. The strain rate range is from 1.7×10^{-3} to 4×10^{3} s^{-1}.

In Figure 7, similar characteristics can be found in the stress-stain curve of the CMDB propellant at a wide range of strain rates: initial linear elasticity, then strain hardening, and the effect of strain hardening increases with the strain rate. These characteristics show the substantial ductile behavior of the CMDB propellant at a wide range of strain rates. Furthermore, the mechanical properties of the CMDB propellant are strain-rate dependent. Moreover, the yield stress of the CMDB propellant increases with increasing strain rate. These characteristics should be considered in the developed constitutive model.

The result of uniaxial compression tests of the CMDB propellant shown in Figure 7 was used to fit by formula (3). The nonlinear least square regression model was used during the fitting process to get the minimal value of the objective function. The objective function is

$$F(x) = \sum_{\dot{\varepsilon}}^{m} \sum_{\varepsilon}^{n} (\sigma_s(x) - \sigma_t)^2. \tag{5}$$

Table 4: Experimental conditions from low to high strain rates of compression tests.

Test type	Low strain rate	Intermediate strain rate	High strain rate
Testing device	Universal testing machine	Hydraulic testing machine	Split Hopkinson pressure bar
Average loading speed/launch the pressure	2, 200 (mm/min)	20, 200 (mm/s)	0.03, 0.1(long) 0.12 (short) (MPa)
Engineering strain rate (s^{-1})	1.7×10^{-3}, 1.7×10^{-1}	1, 10	1000, 2200, 4000

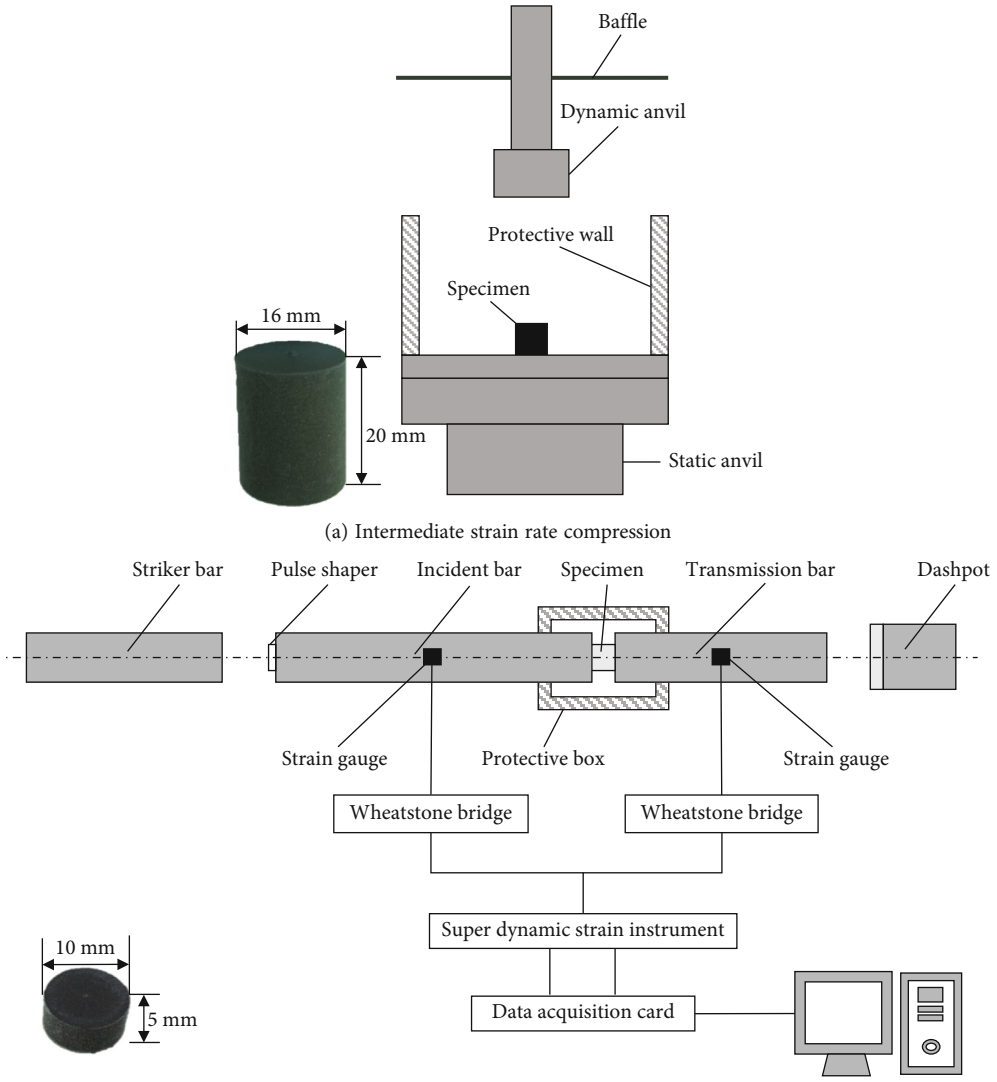

(a) Intermediate strain rate compression

(b) High strain rate compression

Figure 6: Schematic representation of the compression test equipment and specimens.

m is the number of strain rates; n is the number of data points in the single strain rate; x is an unknown parameter in the Prony series; σ_s is the fitting stress; and σ_t is the test stress corresponding to the present strain rate and strain. Table 5 shows the Prony series fitted from CMDB propellant uniaxial compression test data. Figure 8 shows the comparison of the strain–stress curves predicted by the developed constitutive model and those obtained by tests. The results calculated by the developed constitutive model and the test results show good agreement.

3.2. Mechanical Response of Propellant Grain. By using the developed constitutive model, the dynamic collision process between the case and the propellant grain under a vibration load of 20 Hz and an amplitude of 1 mm is simulated. In this section, the radial gap size is set to 5 mm, and the axial gap size is set to 1 mm.

As illustrated in Figure 9, when the motor moves with a cosine function, the motor case and the propellant grain will collide periodically. It should be noted that the stress on the bottom or the top surface of the propellant grain changes

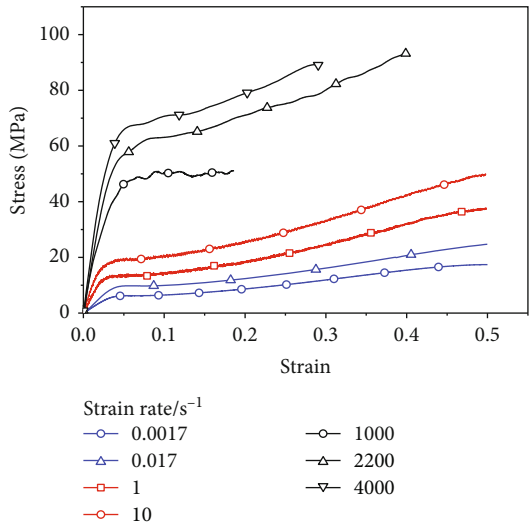

Figure 7: Stress–strain curve of wide strain rate compression.

Table 5: Parameters of $E(t)$ in equation (2).

Parameters (i)	1	2	3	4	∞
E_i/MPa	833.94	1117.36	434.91	299.31	150
θ_i/s	1×10^{-6}	1×10^{-5}	0.001	0.1	∞

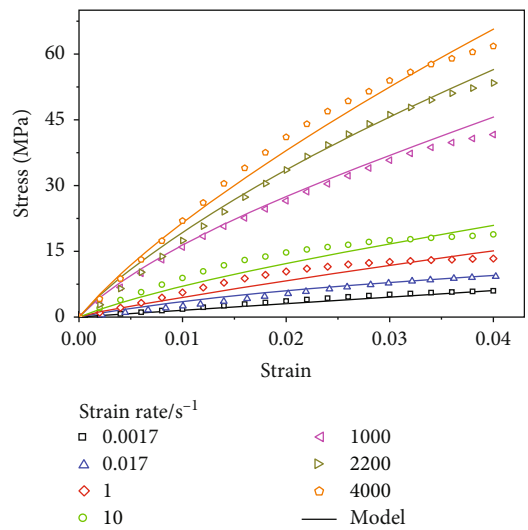

Figure 8: Stress–strain curve of the experimental and fitting data.

over time and is not strictly sinusoidal periodic. Figure 10 shows the maximum stress appears at the first third or fourth collision between the grain and the case; then, the stress decreases gradually and tends to a stable periodic value after 3 collisions.

The maximum radial displacement distribution of the grain is illustrated in Figure 11. The maximum radial displacement of the top surface is 6.13×10^{-3} mm. The maximum radial displacement of the bottom surface is 7.13×10^{-3} mm.

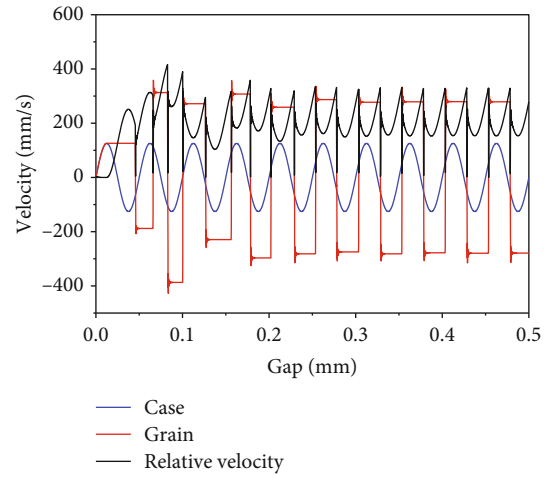

Figure 9: Velocity curve of the motor case and propellant grain.

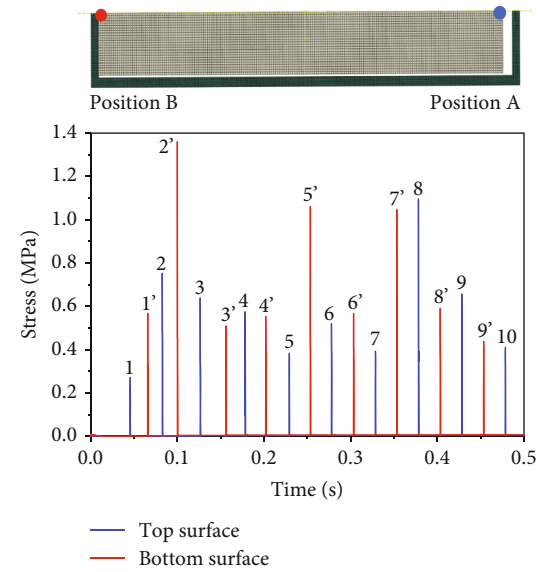

Figure 10: Stress variation versus time of the top (position B) and bottom (position A) of the propellant grain.

As the radial gap of the case and grain is 1 mm, the radial deformation of the grain is far less than the width of the radial gap, so the grain was not in contact with the case during the collision. This is crucial to avoid friction ignition induced by the collision between the grain and the motor case.

During the first collision of the grain and case, the von Mises stress distribution variation versus time is shown in Figure 12. The first collision between the grain and case starts at 45.6 ms and ends at 46.2 ms. The total interaction time of the collision time is approximately 0.6 ms, indicating that the instantaneous collision time is very short. During the collision process, the stress wave propagates in the grain quickly. The maximum stress points are located at the center of the top and bottom surfaces of the grain. According to our calculation, the maximum stress at the center of the top surface is 3.0 MPa, and the maximum stress at the center of the

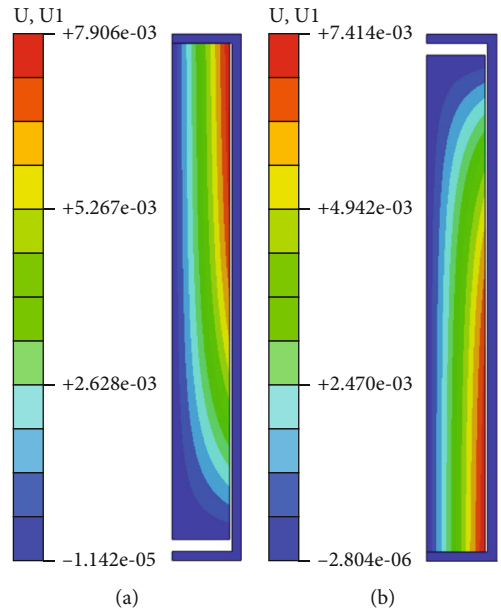

Figure 11: Maximum radial displacement distribution of the propellant grain: (a) top surface of the grain and (b) bottom surface of the grain.

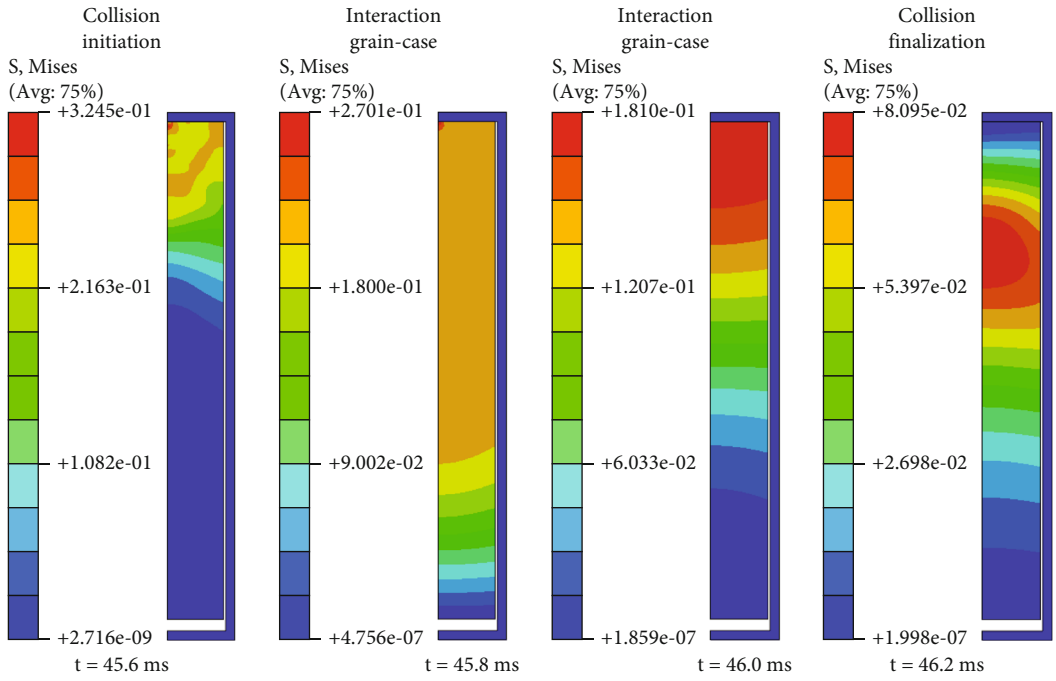

Figure 12: The von Mises stress distribution variation of the grain during the first collision.

bottom surface is 3.6 MPa. Therefore, the center of the bottom and top surfaces of the grain are the danger points.

During the first collision of the grain and case, the strain distribution of the propellant grain is shown in Figure 13. It can be found that the maximum strain points are located at the center of the contact surfaces between the grain and case. The maximum strain at the center of the top surface is 7.66×10^{-4}, and the maximum strain at the bottom surface is 9.83×10^{-4}. It should be noted that in our simulation, the effect of friction is not considered. If the friction effect between the grain and the case is considered, the calculated von Mises stress will possibly decrease due to the limiting action of friction on the grain along the radial direction.

3.3. Effect of the Gap Size. To study the effect of the gap size on the mechanical response of the propellant grain, simulations are performed by changing the gap size to 0 mm, 0.3 mm, π/2 − 1 mm, 1 mm, 2 mm, 3 mm, π mm, 4 mm, 5 mm, 3/2 π +

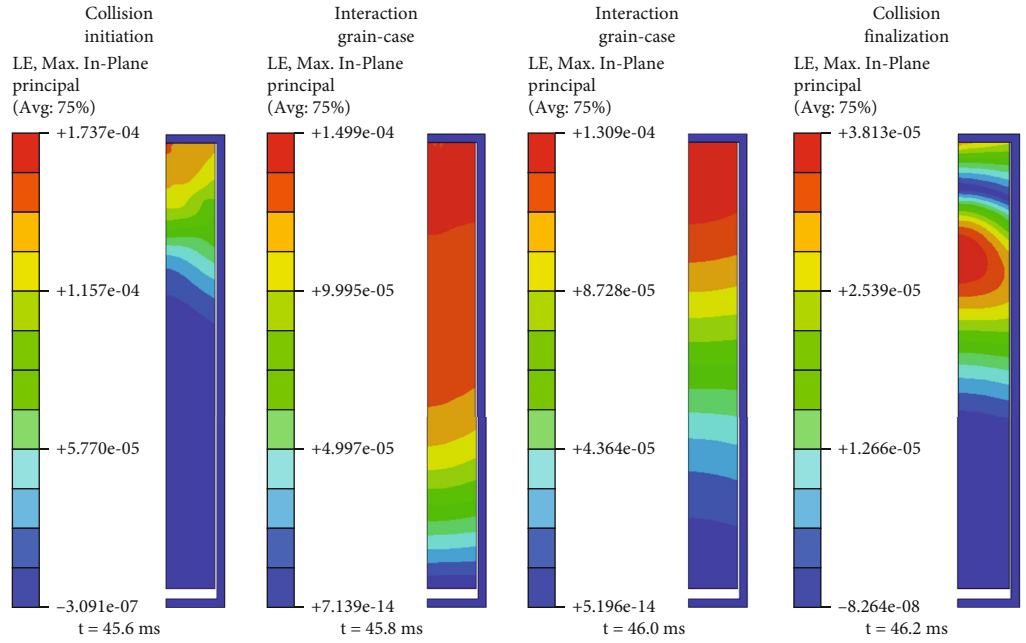

Figure 13: Strain distribution variation of the grain during the first collision.

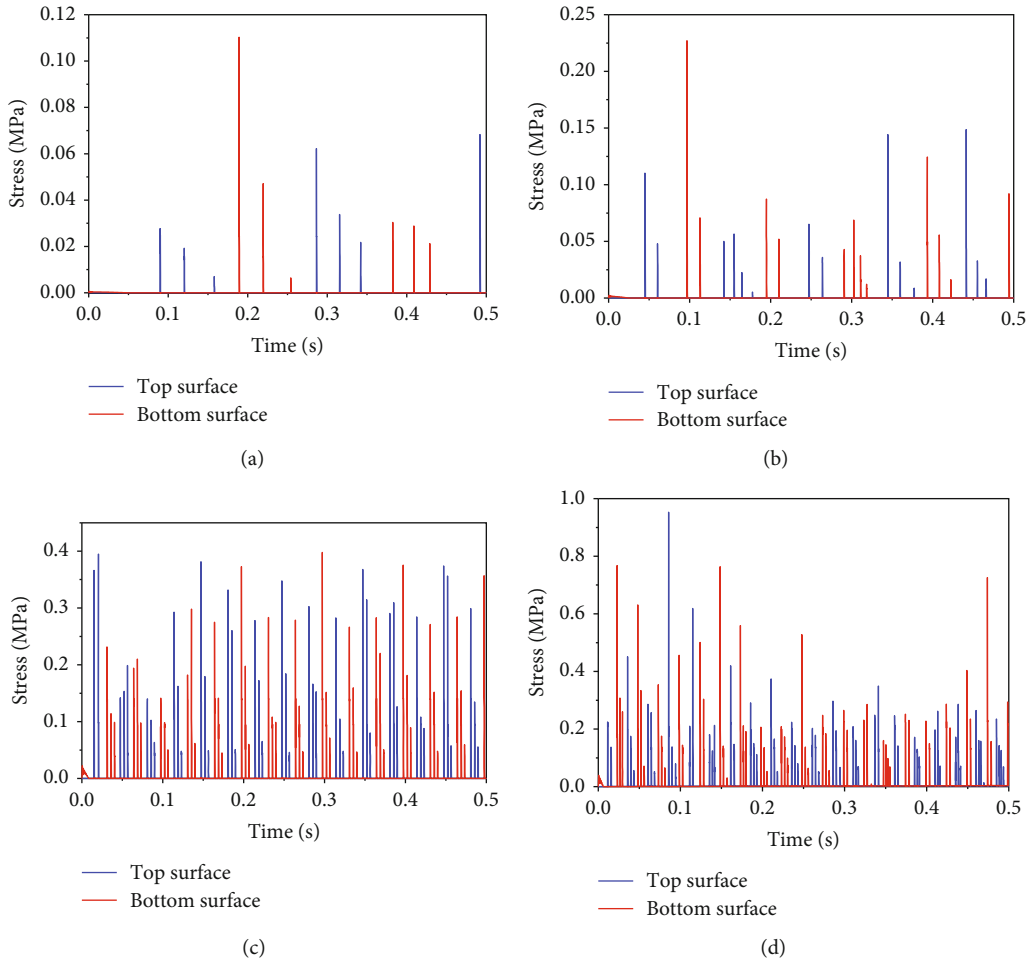

Figure 14: Stress variation versus time of the top (position A) and bottom (position B) of the propellant grain with different vibration frequencies of (a) 5 Hz, (b) 10 Hz, (c) 30 Hz, and (d) 40 Hz.

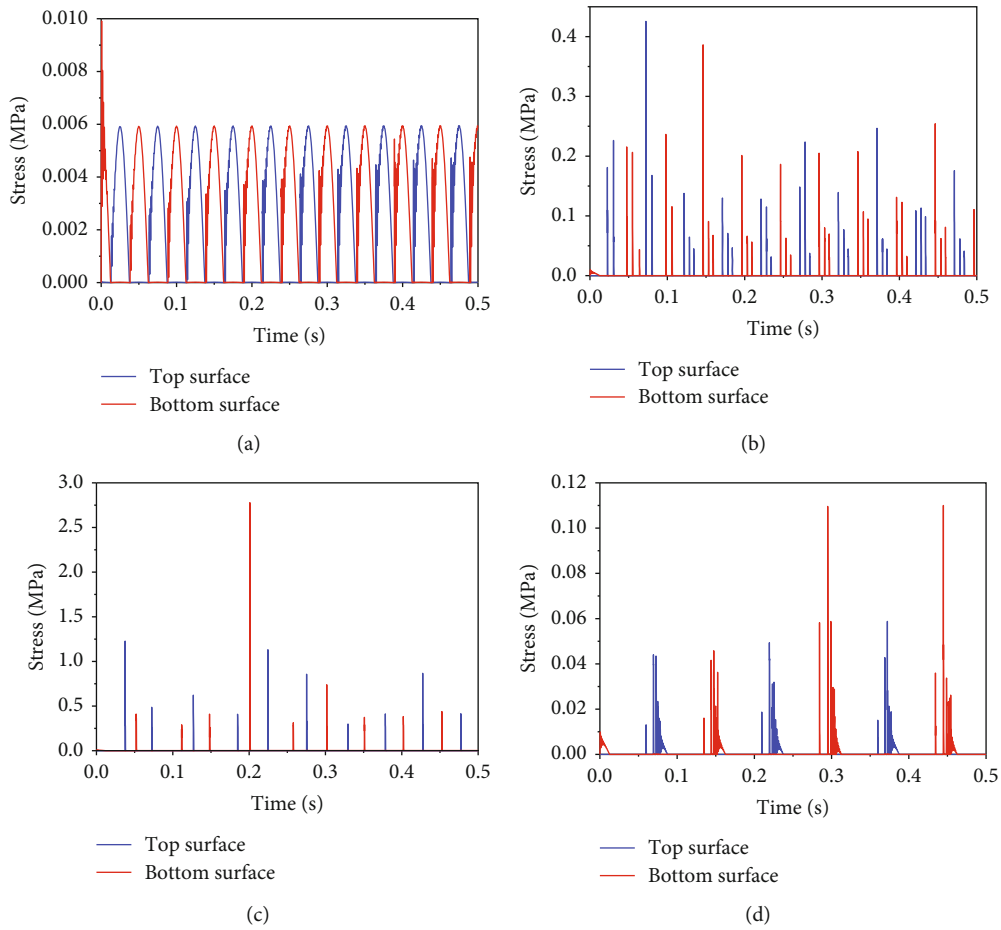

Figure 15: Stress variation versus time of the top (position A) and bottom (position B) of the propellant grain with different radial gap sizes of (a) 0 mm, (b) 0.3 mm, (c) π mm, and (d) 2π mm.

1 mm and 2π mm with the same vibration load of frequency of 20 Hz and amplitude of 1 mm.

Figure 14 illustrates the stress variation of the top and bottom of the propellant grain with different radial gap sizes. This shows that the stress value has a significant dependency on the gap size. When there is no gap between grain and case, i.e., there is no relative motion between them. The stress value varies synchronously with the vibration load, and the stress variation is mainly due to the stress wave propagation inside the grain. The result is shown in Figure 15(a). The maximum stress value is small, with a value of approximately 0.006 MPa. When the gap size increases, the stress value increases dramatically due to the collision between the propellant and the case. As the collision strength is mainly dependent on the impact velocity, when the gap size increases, the relative velocity increases, yielding higher stress values, which are shown in Figures 15(b) and 15(c). Meanwhile, as the motion velocity of the motor case follows a sinuous function, when the gap size reaches 2π, the case and the grain move in the same direction, leading to a small relative velocity at the time of the collision. Therefore, the maximum stress value becomes tiny, as shown in Figure 15(d).

The maximum stresses of the top and bottom of the grain at the different gas sizes are shown in Figure 16. The

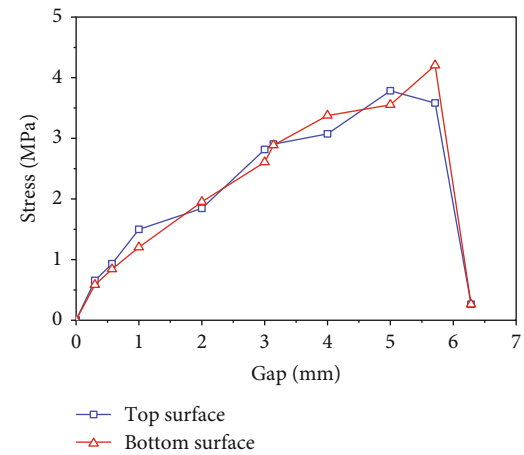

Figure 16: Gap-stress curves of the top and bottom surfaces.

maximum stress of the grain increases gradually with increasing gap size. When the gap is 6 mm, the maximum stress value is 3.55 MPa. When the gap is 2π mm, at the first collision, the relative velocity is 0 between the grain and the case. Therefore, the maximum stress value decreases sharply with a maximum value of 0.30 MPa, which is close to the

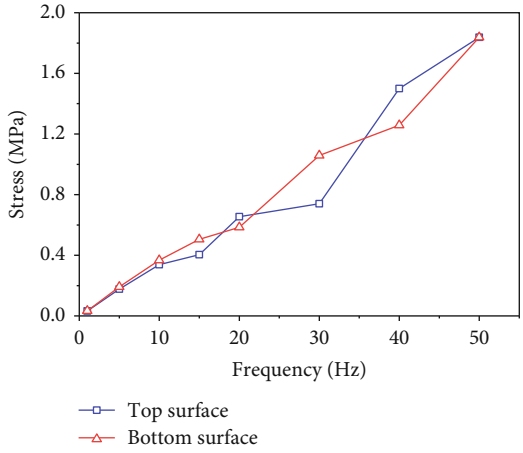

Figure 17: Frequency-stress curve.

case in which there is no gap between the propellant and the motor case.

3.4. Effect of Vibration Frequency. To study the effect of the vibration frequency on the mechanical response of the propellant grain, simulations are performed by changing the vibration frequency from 1 Hz to 50 Hz with the same gap size of 0.3 mm and amplitude of 1 mm.

Figure 14 shows the stress variation of the center points of the top and bottom surfaces at different vibration frequencies. With increasing frequency, the number of collisions of the grain and the case increases, and the collision period is shortened. Figure 17 shows the frequency-stress curves. This figure shows that with increasing frequency, the maximum stress of the grain also increases.

4. Conclusion

Based on the low, intermediate, and high strain rate uniaxial compression measurements of the CMDB propellant, a developed constitutive model which is linear viscoelastic was established. The mechanical response of a cartridge-loaded CMDB propellant grain with an axial gap under a vibration load was simulated and analyzed. The effects of the gap size and the vibration frequency on the response of the propellant grain under vibration loading were discussed. The main conclusions are as follows:

(i) The mechanical properties of the CMDB propellant have a strong strain rate dependency. It exhibits an initial linear elasticity, then strain hardening, and the effect of strain hardening increases with a higher strain rate

(ii) Due to the existence of the axial gap between the case and the grain, the grain collided with the case during the periodic movement of the case. Due to the existence of the gap, the stress value of the propellant increased significantly compared with the situation without radial gaps

(iii) By analyzing the stress and strain distribution of grains in the process of vibration, it is found that the top and bottom of the grain are dangerous positions. Moreover, as the gap size increases, the stress of the propellant grain first increases and then decreases. There exists a gap size that makes the grain obtain the maximum stress value. As the vibration frequency increases, the stress of the grain also increases

Data Availability

Data are available within the manuscript.

Conflicts of Interest

The authors declare that they have no conflicts of interest.

References

[1] Y. Coste and J.-M. Gautier, "Strategic missile solid rocket motor cases qualification," in *42nd AIAA/ASME/SAE/ASEE Joint Propulsion Conference & Exhibit*, Sacramento, California, July 2006.

[2] M. Foster, M. Pieczynski, and J. Steinmeyer, "Taurus II poised to fill the emerging medium-class launch vehicle gap," in *AIAA SPACE 2011 Conference & Exposition*, Long Beach, California, September 2011.

[3] W. S. Kennedy, S. M. Kovacic, E. C. Rea, and T. C. Lin, "Solid rocket motor development for land-based intercontinental ballistic missiles," *Journal of Spacecraft and Rockets*, vol. 36, no. 6, pp. 890–901, 1999.

[4] T. Moore and T. Moore, "Solid propulsion enabling technologies and milestones for navy air-launched tactical missiles," in *AIAA Centennial of Naval Aviation Forum "100 Years of Achievement and Progress"*, Virginia Beach, VA, USA, September 2011.

[5] R. Bertacin, F. Ponti, E. Corti, D. Fedele, and A. Annovazzi, "Numerical simulation of the Zefiro 9 performance using a new dynamic SRM ballistic simulator," in *49th AIAA/ASME/SAE/ASEE Joint Propulsion Conference*, San Jose, CA, USA, July 2013.

[6] S. Bianchi, M. Bonnet, F. Serraglia, F. Iasenzaniro, and C. Milana, "Vega solid rocket motors: an overview of 2006-2007 development activities," in *43rd AIAA/ASME/SAE/ASEE Joint Propulsion Conference & Exhibit*, Cincinnati, OH, USA, July 2007.

[7] A. Davenas, *Solid Rocket Propulsion Technology*, Elsevier Ltd., Amsterdam, 1992.

[8] F. Solymosi and J. H. Block, "Catalytic decomposition of $HClO_4$ vapor over CuO by field ion mass spectrometry," *Journal of Catalysis*, vol. 42, no. 1, pp. 173–176, 1976.

[9] W. Ma, N. Wang, X. Sui, S. Li, and K. Xie, "Thermal safety of a gun-launched missile's solid rocket motor under conditions of high environm. temp. and overloaded forces," *Propellants, Explosives, Pyrotechnics*, vol. 43, no. 12, pp. 1277–1286, 2018.

[10] K. Menke, P. Gerber, E. Geissler, G. Bunte, H. Kentgens, and R. Schöffl, "Characteristic properties of an end burning grain with smoke reduced ferrocene containing composite

propellant," *Propellants Explosives Pyrotechnics*, vol. 24, no. 3, pp. 126–133, 1999.

[11] R. Sangtyani, A. Kumar, A. Kumar, and M. Gupta, "Optimization of network forming agents for different types of composite propellant grain," *Central European Journal of Energetic Materials*, vol. 10, no. 3, pp. 409–418, 2013.

[12] R. Lucas, "Propulsion elements for solid rocket motors," in *Solid Rocket Propulsion Technology*, 1993.

[13] N. Gligorijevic, S. Antonovic, S. Zivkovic, B. Pavkovic, and V. Rodic, "Thermal and acceleration load analysis of new 122 mm rocket propellant grain," *Scientific Technical Review*, vol. 66, no. 3, pp. 3–11, 2016.

[14] W. G. Andrews and T. J. Kirschner, "Heat-sterilizable solid propellant motor designs for interplanetary missions," *Journal of Spacecraft and Rockets*, vol. 4, no. 5, pp. 663–668, 1967.

[15] R. A. Heller and M. P. Singh, "Thermal storage life of solid-propellant motors," *Journal of Spacecraft and Rockets*, vol. 20, no. 2, pp. 144–149, 1983.

[16] G. T. Gray, W. R. Blumenthal, C. P. Trujillo, and R. W. Carpenter, "Influence of temperature and strain rate on the mechanical behavior of Adiprene L-100," *Journal de Physique IV*, vol. 7, no. C3, pp. C3-523–C3-528, 1997.

[17] D. Zhou, X. Liu, X. Sui, Z. Wei, and N. Wang, "Effect of prestrain aging on the damage properties of composite solid propellants based on a constitutive equation," *Propellants, Explosives, Pyrotechnics*, vol. 42, no. 4, pp. 430–437, 2017.

[18] O. Yılmaz, B. Kuran, and G. O. Özgen, "Reliability assessment of solid-propellant rocket motors under storage and transportation loads," *Journal of Spacecraft and Rockets*, vol. 54, no. 6, pp. 1356–1366, 2017.

[19] C. T. Liu, "Crack growth behavior in a solid propellant," *Engineering Fracture Mechanics*, vol. 56, no. 1, pp. 127–135, 1997.

[20] C. W. Fong and R. C. Warren, "The effect of filler particle size and orientation on the impact fracture toughness of a highly filled plasticized polymeric material," *Journal of Materials Science*, vol. 20, no. 9, pp. 3101–3110, 1985.

[21] R. C. Warren, "Impact fracture behaviour of double-base gun propellants," *Journal of Materials Science*, vol. 20, no. 9, pp. 3131–3140, 1985.

[22] C. Sun, J. Xu, X. Chen, J. Zheng, Y. Zheng, and W. Wang, "Strain rate and temperature dependence of the compressive behavior of a composite modified double-base propellant," *Mechanics of Materials*, vol. 89, pp. 35–46, 2015.

[23] R. Zalewski and T. Wolszakiewicz, "Analysis of uniaxial tensile tests for homogeneous solid propellants under various loading conditions," *Gastroenterology*, vol. 144, no. 1, article S-1111, 2011.

[24] N. Gligorijevic, S. Zivkovic, N. Kovacevic et al., "Analysis of viscoelastic behavior of a filled elastomer under action of different loads," *Chemical Industry*, vol. 71, no. 4, pp. 307–317, 2017.

[25] L. Yang, K. Xie, J. Pei, X. Sui, and N. Wang, "Compressive mechanical properties of HTPB propellant at low, intermediate, and high strain rates," *Journal of Applied Polymer Science*, vol. 133, no. 23, 2016.

[26] N. Gligorijevic, S. Zivkovic, V. Rodic et al., "Reliability of solid rocket propellant grain under simultaneous action of multiple types of loads," *Scientific Technical Review*, vol. 66, no. 4, pp. 8–14, 2016.

[27] D. Bynum Jr., "Vibration-test evaluation of an ULLAGE solid-propellant rocket motor," *Experimental Mechanics*, vol. 10, no. 2, pp. 57–63, 1970.

[28] E. Osborne, R. Light, D. Hardy, and M. Steele, "Solid rocket motor random vibration," in *37th Joint Propulsion Conference and Exhibit*, Salt Lake City, UT, USA, July 2001.

[29] H.-U. Oh, T.-G. Kim, S.-H. Han, and J. Lee, "Verification of MEMS fabrication process for the application of MEMS solid propellant thruster arrays in space through launch and on-orbit environment tests," *Acta Astronautica*, vol. 131, pp. 28–35, 2017.

[30] S. Y. Ho, "Viscoelastic response of solid rocket motor components for service life assessment," *Journal of Materials Science*, vol. 32, no. 19, pp. 5155–5161, 1997.

[31] Y. Kohsetsu, "Simplified vibration model of solid-rocket motor coupled with solid propellant," *Journal of Spacecraft and Rockets*, vol. 42, no. 5, pp. 936–942, 2005.

[32] R. Kunz, "Characterization of solid propellant for linear cumulative damage modeling," in *45th AIAA/ASME/SAE/ASEE Joint Propulsion Conference & Exhibit*, Denver, Colorado, 2009.

[33] Z. Weiyao, T. Xiaozhen, D. Tianbao, W. Wenlong, and L. Wei, "Fatigue lifetime estimation of the solid rocket motor charge by road roughness loads on mechanical methods," in *2016 7th International Conference on Mechanical and Aerospace Engineering (ICMAE)*, London, UK, July 2016.

[34] Y. Cao, W. Huang, and J. Li, "*Effect of Ambient Vibration on Solid Rocket Motor Grain and Propellant/Liner Bonding Interface*," *AIP Conference Proceedings*, vol. 1839, no. 1, article 020078, 2017.

[35] W. D. Huang and L. P. Zhang, "Stress and strain analysis of SRM based on monitored shipboard service environment," *Applied Mechanics & Materials*, vol. 275-277, pp. 731–735, 2013.

[36] C. Fang, X. Shen, K. He et al., "Application of fractional calculus methods to viscoelastic behaviours of solid propellants," *Philosophical Transactions of the Royal Society A: Mathematical, Physical and Engineering Sciences*, vol. 378, no. 2172, article 20190291, 2020.

[37] X. Tong, J. Xu, I. Doghri, M. I. El Ghezal, A. Krairi, and X. Chen, "A nonlinear viscoelastic constitutive model for cyclically loaded solid composite propellant," *International Journal of Solids and Structures*, vol. 198, pp. 126–135, 2020.

[38] W. Chen, B. Zhang, and M. J. Forrestal, "A split Hopkinson bar technique for low-impedance materials," *Experimental Mechanics*, vol. 39, no. 2, pp. 81–85, 1999.

[39] E. D. H. Davies and S. C. Hunter, "The dynamic compression testing of solids by the method of the split Hopkinson pressure bar," *Journal of the Mechanics and Physics of Solids*, vol. 11, no. 3, pp. 155–179, 1963.